LETTER Communicated by Emilio Salinas

Higher-Order Statistics of Input Ensembles and the Response of Simple Model Neurons

Alexandre Kuhn
kuhn@biologie.uni-freiburg.de
Ad Aertsen
aertsen@biologie.uni-freiburg.de
Stefan Rotter
rotter@biologie.uni-freiburg.de
Neurobiology and Biophysics, Biology III, Albert-Ludwigs-University, D-79104 Freiburg, Germany

Pairwise correlations among spike trains recorded *in vivo* have been frequently reported. It has been argued that correlated activity could play an important role in the brain, because it efficiently modulates the response of a postsynaptic neuron. We show here that a neuron's output firing rate critically depends on the higher-order statistics of the input ensemble. We constructed two statistical models of populations of spiking neurons that fired with the same rates and had identical pairwise correlations, but differed with regard to the higher-order interactions within the population. The first ensemble was characterized by clusters of spikes synchronized over the whole population. In the second ensemble, the size of spike clusters was, on average, proportional to the pairwise correlation. For both input models, we assessed the role of the size of the population, the firing rate, and the pairwise correlation on the output rate of two simple model neurons: a continuous firing-rate model and a conductance-based leaky integrate-and-fire neuron. An approximation to the mean output rate of the firing-rate neuron could be derived analytically with the help of shot noise theory. Interestingly, the essential features of the mean response of the two neuron models were similar. For both neuron models, the three input parameters played radically different roles with respect to the postsynaptic firing rate, depending on the interaction structure of the input. For instance, in the case of an ensemble with small and distributed spike clusters, the output firing rate was efficiently controlled by the size of the input population. In addition to the interaction structure, the ratio of inhibition to excitation was found to strongly modulate the effect of correlation on the postsynaptic firing rate.

1 Introduction

The brain consists of a huge number of neurons that are heavily interconnected. These cells interact by producing rapid depolarizations of their membrane, the action potentials (spikes) that are propagated along the axon and excite or inhibit postsynaptic neurons by inducing postsynaptic potentials (PSPs). The integration of PSPs can bring the postsynaptic neurons, in turn, to fire a spike.

Such interactions within the neuronal network lead to temporal correlations between spike trains of different neurons. Pairwise correlations of spike trains are routinely observed in virtually all regions of the brain. They have been related to the representation of sensory information (DeCharms & Merzenich, 1996) and motor behavior (Baker, Spinks, Jackson, & Lemon, 2001), but also to more abstract processing levels (Steinmetz et al., 2000; Salinas & Sejnowski, 2001). The effect of correlated synaptic input on the neuronal response has been investigated in several recent theoretical and numerical studies (Feng & Brown, 2000; Salinas & Sejnowski, 2000; Svirskis & Rinzel, 2000; Feng & Zhang, 2001; Stroeve & Gielen, 2001). They showed that temporal correlation can have a tremendous effect on the rate and variability of the output of model neurons.

Pairwise correlations are generally used to characterize the statistical dependence of parallel spike trains. However, as pointed out, for example, by Bohte, Spekreijse, and Roelfsema (2000), an ensemble of spike trains is not completely described by pairwise interactions. Thus, the effect of pairwise correlation cannot be studied without also taking into account correlations among three or more spike trains (i.e., higher-order interactions). This point is illustrated by the following example. Under the general assumption that only the timing of presynaptic spikes and not their form is important, we can model series of incoming spikes as point processes (Tuckwell, 1988; Cox & Isham, 1980). A presynaptic ensemble of N spike trains can then be thought of as N parallel point processes. We define an interaction as the occurrence of simultaneous spikes in different spike trains. The interactions can be classified as second, third, ..., Nth-order, corresponding to clusters of $2, 3, \ldots, N$ simultaneous spikes. For simplicity, we assume that the ensemble is homogeneous, that is, the firing rates of all spike trains are identical and, similarly, the rates of second, third, ..., Nth-order interactions are identical for any subset of $2, 3, \ldots, N$ spike trains picked from the ensemble. We now consider a homogeneous ensemble of N parallel spike trains where all spikes are associated with pairwise (second-order) interactions: there are no interactions of order 3 or higher, nor are there isolated spikes, that is, spikes in one spike train without a counterpart in another one. If κ is the rate of each second-order interaction, the discharge rate r of an individual spike train is $r = (N-1)\kappa$. The correlation coefficient between two point processes in a homogeneous system is the rate of interactions with simultaneous spikes on both processes, divided by the

discharge rate of an individual process (see appendix A). Thus, in the case of an ensemble with only second-order interactions, the correlation coefficient is $c = 1/(N-1)$. It is approximately inversely proportional to the number of presynaptic inputs. For $N = 100$ correlated spike trains, the correlation coefficient will be about 10^{-2}. Stronger pairwise correlations can be obtained only by introducing higher-order interactions. A single third-order interaction (or triplet), for instance, contributes to the pairwise correlations in three pairs of spike trains, while introducing only one spike per process. The same second-order interaction is obtained by having one pair of spikes in each of the three pairs of spike trains. This results in two spikes in each single process, that is, twice as many as in the triplet case, which results in a halved correlation coefficient.

In a homogeneous high-dimensional system, certain combinations of rates and pairwise correlations thus imply the existence of higher-order interactions. Biological neural networks are typically not homogeneous (in the sense defined above), but very little is known about their actual interaction structure. The assessment of the statistical significance of simultaneous events across more than two neurons is a nontrivial problem. Different statistical methods have been proposed (Martignon, von Hasseln, Grün, Aertsen, & Palm, 1995; Martignon et al., 2000; Gütig, Aertsen, & Rotter, 2002).

Here, we report on a study of the effects of higher-order interactions on the response of model neurons. Specifically, we constructed two different spike train ensembles and compared their effects on the response of a firing-rate (FR) neuron model and a conductance-based leaky integrate-and-fire (IF) model. For both neuron models, we assessed the effects of the pairwise correlation in the input on the output firing rate of the neuron. Analytical results were derived for the FR neuron. Preliminary results have been presented elsewhere (Kuhn, Rotter, & Aertsen, 2002).

2 Two Models for Correlated Neuronal Populations

The realization $x(t)$ of a stochastic point process consists of a sequence of points in time $\ldots, t_k, t_{k+1}, \ldots$ that can be represented by a pulse train,

$$x(t) = \sum_k \delta(t - t_k),$$

where $\delta(t)$ is the Dirac delta function. To reduce the number of parameters defining the input ensemble, we model spike trains as parallel Poisson point processes with homogeneous interaction structures. Moreover, we restrict our treatment to instantaneous statistical dependence, that is, the interaction among spike trains originates from simultaneous spikes only.

2.1 Single Interaction Process Model. The single interaction process (SIP) model was motivated by results of Deppisch et al. (1993) and Bohte et al. (2000). They simulated a network of integrate-and-fire neurons and

observed that it could show periods of random looking, unsynchronized neuronal activities, but also population bursts, with almost all neurons firing synchronously. The SIP model is defined as follows. First, a single realization $w_u(t)$ of a Poisson process with stationary rate α is generated. Each process $x_i(t)$ in a set of N spike trains is then defined by

$$x_i(t) = w_u(t) + w_i(t) \quad (i = 1, 2, \ldots, N),$$

where $w_i(t)$ is an independent realization of a Poisson process with rate β. The superposition of independent Poisson processes is again a Poisson process with a rate equal to the sum of the individual rates (see Cox & Isham, 1980). Thus, the rate of $x_i(t)$ is

$$r = \alpha + \beta.$$

Figure 1A shows the realization $w_u(t)$ (top) that is copied into each individual spike train $x_i(t)$ (bottom), introducing a statistical dependence between them. We characterized the statistical dependence between two spike trains by the count correlation coefficient,

$$c = \alpha/(\alpha + \beta).$$

Note that the ensemble model is completely constrained by the rate r and the pairwise count correlation coefficient c. The relations $\alpha = rc$ and $\beta = r(1-c)$ are used for the numerical simulation of a set of spike trains with given rate and given pairwise correlation. In the literature, the pairwise dependence is frequently expressed by the cross-correlation. The cross-correlation function $R(\Delta t)$ of two spike trains $x_i(t)$ and $x_j(t)$ is

$$R(\Delta t) = \alpha\delta(\Delta t) + (\alpha + \beta)^2.$$

A derivation of the cross-correlation function and the count correlation coefficient is presented in appendix A.

When using the SIP model as input to a point neuron, all individual spike trains $x_i(t)$ are summed up. The compound process can, in turn, be decomposed into two independent processes: a Poisson process with rate α, in which each point accounts for N simultaneous spikes, and a Poisson process of rate $N\beta$, resulting from the sum of all independent realizations $w_i(t)$. The dependence between spike trains in the SIP model is thus described by a single interaction process (of order N). We can write

$$\sum_i x_i(t) = \sum_i [w_u(t) + w_i(t)] = N w_u(t) + \sum_i w_i(t).$$

The decomposition into two independent processes greatly facilitates the analysis of the neuronal response. This model of correlated spike trains also appears in Feng and Brown (2000) and Stroeve and Gielen (2001).

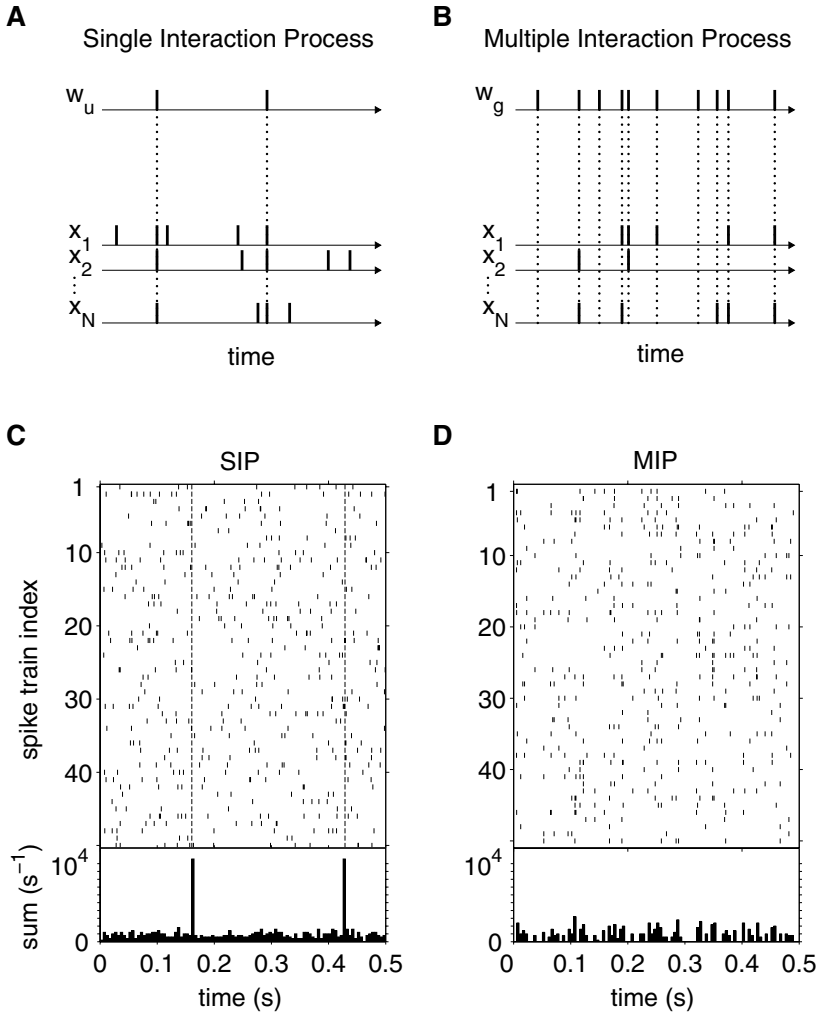

Figure 1: Two models of spike train ensembles with identical rates and pairwise correlations but different higher-order statistics. (A) The single interaction process (SIP) model. Each spike train $x_i(t)$ of the ensemble is composed of a fixed realization $w_u(t)$ of a Poisson process with rate α and an independent realization of a Poisson process with rate β. (B) The multiple interaction process (MIP) model. Each spike train $x_i(t)$ is realized by randomly deleting spikes from a fixed realization $w_g(t)$. The generating process is a realization of a Poisson process with rate γ. (C) Fifty spike trains with a rate of 20 spikes per second and pairwise correlation coefficient 0.1, generated according to the SIP model. Their summed activity is shown below (bin size 5 ms). (D) Fifty spike trains with the same rate and pairwise correlation as in *A*, but generated according to the MIP model.

2.2 Multiple Interaction Process Model. In the second model of a spiking population, the interaction structure is composed of spike clusters involving only subsets of the spike trains. The multiple interaction process (MIP) model is constructed as follows. Each individual spike train is a thinned version (Cox & Isham, 1980) of one and the same realization $w_g(t)$ of a Poisson process. Individual spike trains $x_i(t)$ are thus produced by random deletions of pulses in $w_g(t)$. The deletions are independent. The thinning process is repeated for all spike trains in the ensemble. If the rate of $w_g(t)$ is γ and the probability of deletion is $(1 - \epsilon)$, then the rate of each individual spike train is

$$r = \gamma\epsilon.$$

Figure 1B shows the generating process $w_g(t)$ (top) and the resulting correlated spike trains $x_1(t), \ldots, x_N(t)$ (bottom). Note that the pulses in each individual spike train are Poisson (Snyder & Miller, 1991). The count correlation coefficient is

$$c = \epsilon.$$

Again, the rate r and correlation coefficient c together completely constrain the model, and the relations $\epsilon = c$ and $\gamma = r/c$ are used for the numerical simulation of the ensemble of spike trains. The cross-correlation function of any two spike trains $x_i(t)$ and $x_j(t)$ is

$$R(\Delta t) = \gamma\epsilon^2\delta(\Delta t) + (\gamma\epsilon)^2.$$

The derivation of the cross-correlation function and the count correlation coefficient is again given in appendix A.

The sum of the N individual spike trains results in a pulse train similar to the generating realization $w_g(t)$, but with each pulse scaled differently. The scalar amplitude n represents the number of (synchronous) spikes at this point in time. As the deletion of a certain pulse in $w_g(t)$ occurs with a fixed probability and is independent for each of the N individual spike trains, the number n follows a binomial distribution:

$$n \sim \mathrm{B}(n; \epsilon, N) = \binom{N}{n} \epsilon^n (1 - \epsilon)^{N-n}.$$

The scalar n is independent for each point in the compound process. The sum process can thus be decomposed into $N + 1$ independent Poisson processes (Snyder & Miller, 1991), each process containing only points with identical multiplicity. Such a process is called an interaction process of order n, with $n \in \{0, 1, \ldots, N\}$. Evidently, the rate of the interaction process of order n is $\gamma\mathrm{B}(n; \epsilon, N)$.

Figures 1C and 1D show realizations of an ensemble of 50 spike trains, generated according to the SIP and the MIP model, respectively. In both

cases, the individual input rate r and the count correlation coefficient c were identical ($r = 20$ spikes per second, $c = 0.1$). The compound activity of all spike trains is shown below the spike rasters. Although any single spike train, as well as any pair of spike trains picked from the two ensembles, would be statistically indistinguishable, the population activity is clearly different for both models.

3 Results

The effects of both ensemble models were tested on two neuron models. To reduce the complexity of the input, we first focused on a simplified setting. We assume the input population to be composed of two subpopulations, one excitatory and one inhibitory, with the same size and rate of the excitatory and the inhibitory populations. The excitatory presynaptic spike trains were correlated, generated according to the SIP or the MIP model, whereas the inhibitory presynaptic spike trains were modeled as independent Poisson processes. We assessed the influence of the input parameters, and in particular of the excitatory pairwise correlation, on the mean output rate of two types of model neurons: the FR neuron and the conductance-based leaky IF neuron. The output of the FR neuron is represented by a continuous function of time, the instantaneous firing rate of the neuron, and could be treated analytically. The response of the IF neuron was studied by means of numerical simulations. In addition, the latter model was studied for inputs with different proportions of excitation and inhibition.

3.1 Response of the Firing Rate Neuron. The continuous FR neuron is widely used in neural network studies. Its membrane potential $U(t)$ is described by

$$C\frac{d}{dt}U(t) = -\frac{1}{R}U(t) + I(t), \tag{3.1}$$

with C the membrane capacitance, R the membrane resistance, and $I(t)$ the input current. The membrane potential $U(t)$ is a low-pass version of the input current $I(t)$. The output firing rate $r_o(t)$ of the neuron is given by the activation function, which is assumed to be an instantaneous function of the potential. Here, we used the Heaviside step function $H(x)$,

$$H(x) = \begin{cases} 0 & \text{for } x < 0 \\ 1 & \text{for } x \geq 0. \end{cases} \tag{3.2}$$

In this case, the output rate of the neuron is expressed by

$$r_o(t) = KH(U(t) - \theta), \tag{3.3}$$

where θ represents the threshold and K is a constant with dimension spike per second. Alternatively, a sigmoidal function is often used as activation function. In our case, however, we used the step function because it greatly facilitates the analysis of the neuronal response. Since we are interested only in the qualitative behavior of the output rate, the constant K will not be considered any further, and $r_o(t)$ will be dimensionless.

An example of the response of the membrane potential $U(t)$ to the input described above is shown in Figure 2. Synapses were modeled by current pulses. The PSPs were thus represented by an instantaneous jump of potential (positive or negative, according to the excitatory or inhibitory nature of the synapse), followed by an exponential decay toward rest, with time constant $\tau = RC = 10$ ms. Excitatory and inhibitory PSPs had the same absolute amplitude, fixed at a value of 1. The excitatory and inhibitory input population size was $N = 100$ in this example, and the individual excitatory and inhibitory input firing rate was $r = 20$ spikes per second. The excitatory input was modeled by the SIP model (see Figure 2A), or by the MIP model (see Figure 2B), and the pairwise correlation coefficient was $c = 0.4$, in both cases. Observe that for both input models, the membrane potential shows large depolarizations caused by the occurrence of synchronous excitatory presynaptic spikes. These depolarizing events had, however, different characteristics for both input models, as we will see in more detail in the following.

3.1.1 Amplitude Distribution of the Membrane Potential. The probability density function (pdf) of the amplitude distribution of the membrane potential is represented in Figure 2 next to sample time courses of the membrane potential. The histogram is an estimate generated from a 200 s simulation, with a bin size of 4 (in units of the PSP amplitude). The thick black lines represent an analytical approximation of part of the pdf. As the output rate of the FR neuron is an instantaneous function of the membrane potential, knowledge of the pdf of the potential is sufficient to derive the mean output rate of the neuron. We now describe the main assumptions made to obtain the approximation of the pdf; a full derivation for the potential and the mean output rate is given in appendix B. The approximation of the pdf is based on the decomposition of the input into independent components (cf. section 2) and the use of a classical result of shot noise theory. The membrane potential of a FR neuron can be considered as a filtered point process. Assuming identical synapses, it can be represented by $U(t) = \sum_k h(t - t_k)$, with t_k denoting the times of occurrences of synaptic events and $h(t)$ the impulse response of the filter realized by the synapse and the membrane. For synapses modeled as current pulses, $h(t)$ is simply the impulse response of the membrane, given by

$$h(t) = \begin{cases} 0 & \text{for } t < 0 \\ Ae^{-t/\tau} & \text{for } t \geq 0, \end{cases} \tag{3.4}$$

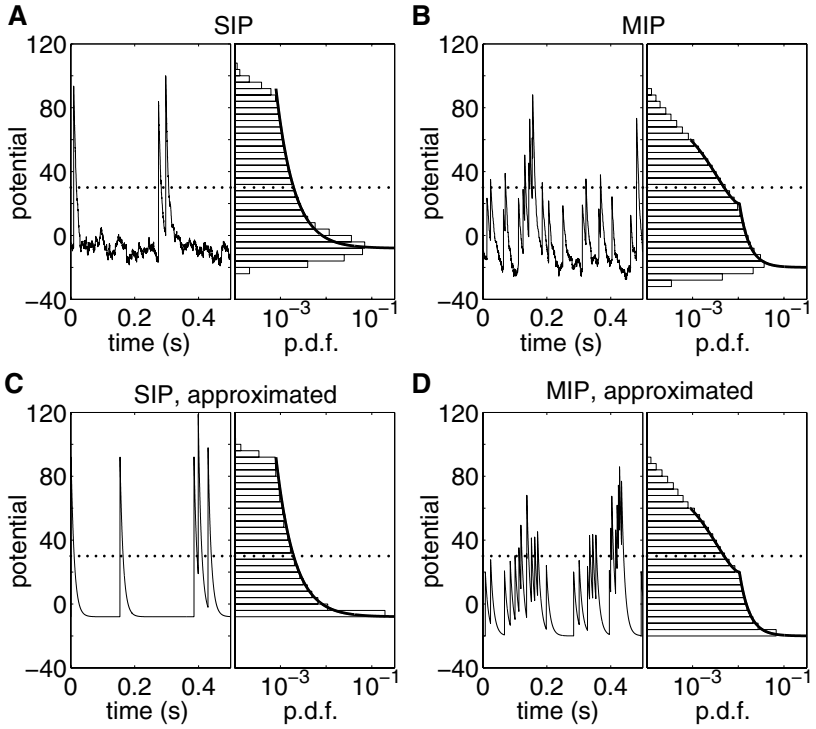

Figure 2: Time course (left) and probability density function (pdf, right) of the membrane potential of the firing rate (FR) neuron. The membrane potential is expressed in units of the PSP amplitude. (A) The excitatory input to the FR neuron consisted of 100 excitatory spike trains, generated according to the SIP model (individual firing rate is 20 spikes per second, pairwise correlation 0.4). The inhibitory input was composed of 100 independent Poisson processes with a rate of 20 spikes per second. The pdf estimated from a 200 s simulation of the membrane potential is shown on the right (histogram with a bin width of 4). A segment of the analytical approximation of the pdf (see text) is overlaid (thick black line). The dotted line indicates the firing threshold. (B) Same input rate and pairwise correlation as in *A*, but using the MIP model for excitatory inputs. (C) Approximation (see text for details) of the membrane potential with the SIP model as excitatory input. The approximation retained the large fluctuations caused by clusters of synchronous input spikes (compare with *A*). The estimated pdf of the approximated membrane potential (from a 200 s simulation of the approximated membrane potential, bar histogram) matched the analytically calculated pdf (thick black line, same as in A). (D) Approximation of the membrane potential using the MIP model for excitatory inputs. Again, the estimated pdf (histogram) matched the analytical expression (thick black line, same as in B).

with A being the postsynaptic potential amplitude and τ the membrane time constant. If the synaptic events follow a Poisson statistics, the filtered process is called a shot noise (Papoulis, 1991). If the rate of the incoming events is large compared to the time constant of the filter, the distribution of membrane potentials is approximately gaussian (see Papoulis, 1991). In the case of our two input models, however, the interaction structure does not admit a normal approximation. The right panels in Figures 2A and 2B show that the membrane potential densities are clearly not gaussian. Gilbert and Pollak (1960) derived an exact expression for the pdf of a shot noise with exponential impulse response. They showed that for $A = 1$ and $\tau = 1$, the shot noise $U(t)$ with underlying rate of pulses $\lambda = 1$, has density

$$P(U) = \begin{cases} e^{-g} & \text{for } 0 \le U < 1 \\ e^{-g}(1 - \log U) & \text{for } 1 \le U < 2, \end{cases}$$

where $g = -\int_0^\infty e^{-t} \log t \, dt$, Euler's constant. In fact, the analytic expression of $P(U)$ changes at $U = 1, 2, 3, \ldots$ The expression for a given segment is derived recurrently from the expression of the preceding segment. The case with parameters A, τ, and λ arbitrary can be extended from the results of Gilbert and Pollak (1960) and is shown in appendix B.

3.1.2 Analytic Approximation of Membrane Potential Distribution. What is the use of this result for the derivation of the membrane potential density of the FR neuron to the SIP and MIP input models? If the proportions of excitation and inhibition are equal (i.e., the input is balanced), the neuron's output firing rate is driven by the fluctuations of the membrane potential above the threshold. Synchronous clusters of input spikes induce large excursions of the membrane potential that are likely to constitute the major contribution to the neuronal output rate. If, in addition, the nonsynchronous input spikes (excitatory or inhibitory) do not significantly contribute to the membrane potential excursions, but only to the mean membrane potential level, we can approximate the membrane potential by the filtered interaction process (i.e., the process with simultaneous spikes), together with a constant membrane potential offset due to the nonsynchronous input spikes. For the input with the SIP model, the interaction process has fixed amplitude N and rate rc, and the nonsynchronous input consists of an excitatory spike train with rate $Nr(1-c)$ and an inhibitory spike train with rate Nr. The resulting mean membrane potential offset is given by Campbell's theorem and amounts to $-Nrc\tau$ (see appendix B). We can write

$$P(U) \approx P_{e_N}(U + Nrc\tau),$$

where the pdf of the potential response to the SIP model is approximated by a shifted version of the pdf of the filtered Nth-order interaction process $P_{e_N}(U)$. The latter can be derived on the basis of Gilbert and Pollak's method.

The rigorous justification of this approximation is given in appendix B. Figure 2C shows an example of the time course of the approximated membrane potential, with the same parameters as in Figure 2A (left panel). Observe that the small fluctuations caused by the nonsynchronous input spikes disappeared, but their mean level was retained.

A similar approximation can be made for input defined by the MIP model. To be able to use the shot noise density directly, we make the additional assumption that the stochastic spike clusters generated by the MIP model can be approximated by the average cluster; we replace the $N + 1$ interaction processes of order 0 to N by a single interaction process of order (amplitude) Nc and rate r/c. The density of the potential response to the MIP model thereby becomes

$$P(U) \approx P_{e_{\vec{n}}}(U + Nr\tau),$$

where $P_{e_{\vec{n}}}(U)$ is the pdf of the filtered average interaction process and $-Nr\tau$ the mean membrane potential offset, caused by the independent inhibitory input. Again, we refer to appendix B for a complete derivation of this result. An example of the time course of the approximated membrane potential response to the input with the MIP model is shown in figure 2D (left panel).

Because of the piecewise expression of the shot noise pdf, the convenience of our approximation depends on the number of segments that must be taken into account. For a membrane's impulse response of amplitude A (see equation 3.4), the expression changes its form at integer multiples of A. For the SIP model (see Figure 2C, right), the neuron's response to a synchronized spike cluster has amplitude N. We used the first segment of the pdf, extending over $[-Nrc\tau, -N(rc\tau - 1)[$. (We use the conventional mathematical notation $x \in [a, b[$ to indicate $a \leq x < b$.) For the parameter set considered here, the approximation of the potential holds for $U \in [-8, 92[$ in units of A. Comparison with the histogram estimated from 200 second simulation of the approximated membrane potential shows an excellent correspondence. For the MIP model (see Figure 2D, right), we used the first two segments. As we reduced the model's interaction structure to the average spike cluster, the neuron's response to a synchronized cluster has amplitude Nc, and the first two segments cover $[-Nr\tau, -N(r\tau - 2c)[$, which corresponds to $[-20, 60[$. Note that the change of the analytic form of the pdf can be recognized from the sharp bend at $U = -N(r\tau - c) = 20$. Again, a numerical estimate from the simulation of the approximated membrane potential (see the histogram in Figure 2D, right) shows excellent correspondence. If we now compare the analytical approximation of the pdf with the pdf estimated from a simulation of the full input model (Figures 2A and 2B, right), the agreement is very good. A small discrepancy can be observed only near the lower bound of the domain considered. There, our approximation neglected the fluctuations due to the nonsynchronous input spikes that spread the membrane potential around the mean value.

3.1.3 Mean Response Rate. We can now consider the mean output rate r_o for the FR neuron,

$$r_o \equiv \mathrm{E}[(r_o(t)] = \int_\theta^\infty P(U)\, dU = 1 - Q(\theta), \tag{3.5}$$

where $Q(x) = \int_{-\infty}^{x} P(U)\, dU$, the cumulative probability distribution function of the membrane potential. We thus obtain an approximation of the mean output rate by integrating over the approximated density, which has to be known between $-\infty$ and θ. In Figure 2, the threshold θ is represented by a dotted line and was set to 30. The number of segments of the pdf that must enter the calculation of r_o is thus determined by the value of the input parameters, the threshold, and the membrane time constant. For the SIP model, an approximation of the mean output rate based on the first segment of the probability distribution is

$$r_o \approx 1 - \left[\widetilde{D}\left(\frac{\theta}{N} + rc\tau\right)^{rc\tau} \frac{1}{rc\tau}\right], \tag{3.6}$$

with $\widetilde{D} = e^{-rc\tau g}/\,\Gamma(rc\tau)$, where $\Gamma(z) = \int_0^\infty t^{z-1}e^{-t}dt$ is the gamma function. It is valid for $-rc\tau \le \theta/N < -(rc\tau - 1)$. For larger θ, additional segments of the distribution have to be included. For the MIP model, the approximation based on the first two segments is given in appendix B in equation B.2.

We used these approximations to study the output rate of the FR neuron in response to both types of input. The input was described by three parameters: the size N of the input population, the rate r of individual inputs, and the correlation coefficient c between any two individual excitatory inputs. N and r were identical for the excitatory and the inhibitory populations. We examined how the input correlation coefficient c influenced the mean output rate r_o of the FR neuron. In addition, we systematically varied N and r. The results are shown in Figure 3. Analytical approximations are represented by thick gray lines, and results obtained by numerical simulations are given by black dots. Figure 3A shows the output rate r_o as a function of the input correlation coefficient c for several input population sizes $N = 40$, 100, 500, 1000 and a fixed input rate of $r = 20$ spikes per second. The SIP model was used as the excitatory input ensemble. For all N, r_o increased monotonically with the correlation coefficient. Indeed, as c grows larger, the rate of occurrence of simultaneous excitatory input spikes, given by rc, increases, and membrane potential excursions above threshold become more frequent, leading to an increase of the mean output rate. Nevertheless, observe that the overall increase of r_o does not scale with N and tends to saturate rapidly for larger input population sizes. In the limit $N \to \infty$, we have

$$r_o \approx 1 - \frac{(rc\tau)^{rc\tau-1}}{\Gamma(rc\tau)} e^{-rc\tau g}.$$

This limit is plotted as a dashed line in Figure 3A. Figure 3B features the output rate of the FR neuron for identical input conditions, with an interaction structure of the excitatory population generated according to the MIP model. For small values of c, the response of the FR neuron showed a considerably stronger dependence on the ensemble size than in the SIP model. For $N = 40$, for instance, the initial increase of r_o was smaller than with the SIP model. By contrast, for $N = 1000$, a small input correlation induced a much larger output rate with the MIP model. For larger N, a further increase of c led to a decrease of r_o. Note that for $c = 1$, both correlated input models are statistically identical, and the responses of the FR neuron were thus the same.

For both the SIP and MIP input models, the analytical approximations of r_o for the FR neuron model were in very good agreement with the simulation results, showing that the assumptions made were appropriate. As hypothesized, the response of the neuron is driven by the occurrence of excitatory spike clusters for the largest part of the correlation range. If c approaches 0, the rate of these synchronous events tends to 0, and the approximate treatment of the SIP model degrades. The reason is that it neglects the contribution of nonsynchronous excitatory input spikes, the rate of which is $Nr(1-c)$, increasing for smaller c. This is shown in the inset of Figure 3A, depicting the output rate of the FR neuron for $c = 0.005, 0.01, \ldots, 0.1$. Whereas the approximation tends to 0, the neuron response to the full SIP input model has nonzero values at $c = 0$, for $N = 1000$. The success of the approximation near $c = 0$ thus critically depends on the values of r and N.

For the response to the MIP model, we limited the approximation to the first two segments of the pdf and thus could not approximate the response of the FR neuron over the whole range of c (see Figure 3B). For small correlation coefficients, the size of the mean synchronous spike cluster Nc is small compared to the threshold, and many segments of the shot noise density must be taken into consideration. The success of the analytical approximation here indicates that the stochastic nature of the size of synchronous clusters does not play a significant role for the mean output rate.

This independence of the stochastic nature of the cluster size allows us to explain the observed effects in terms of the average cluster. For small values of c, the rate r/c of the mean cluster is large. The frequent occurrence of small clusters (with size proportional to c) results in their accumulation in the membrane potential, which drives the potential above threshold θ (see Figure 2B) and increases the output rate. Nevertheless, the rate of occurrence of the synchronous input events decreases with increasing c. The clusters become larger but less frequent with increasing c. If their mean inter-event interval (inverse rate) is smaller than the membrane time constant, they do not accumulate, and the increase of the cluster size cannot compensate for their less frequent occurrence. For a large input population size, these two opposing effects result in a non-monotonic dependence of the output rate on the input correlation (see Figure 3B).

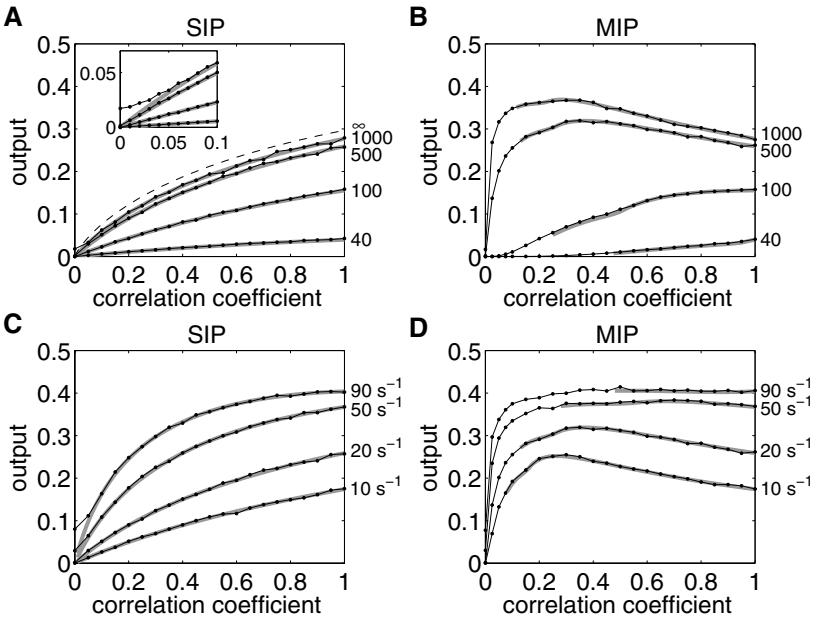

Figure 3: Mean output of the firing rate (FR) neuron as a function of the pairwise correlation coefficient in the population of excitatory inputs, for the two statistical input models. Relative units are used (see text). Thick gray lines are obtained from analytical approximations (see text); the black dots represent the results of simulations (duration 500 s each). (A) The excitation was generated according to the SIP model, and the inhibition was represented by a set of independent Poisson processes. Excitatory and inhibitory population size and rate were identical. The output rate of the FR neuron is shown for different input population sizes ($N = 40, 100, 500, 1000$). The individual input rate was held constant ($r = 20$ spikes per second). The analytically computed output rate of the FR neuron for infinite population size is plotted as a dashed line. Inset: Zoom-in of the graph for low pairwise correlation coefficients ($0 \leq c \leq 0.1$). (B) The excitation was generated according to the MIP model, everything else as in *A*. (C) Same input setting as in *A*, but for a fixed input population size ($N = 500$) and different individual input rates ($r = 10, 20, 50, 90$ spikes per second). (D) The excitation was generated according to the MIP model. Everything else as in *C*. Note that for $c = 0$ and $c = 1$, the SIP and the MIP models coincide.

Figure 3C shows the output rate r_o for a fixed population size of $N = 500$ and for different input rates $r = 10, 20, 50, 90$ spikes per second, with the SIP model being used as excitatory input ensemble. The output rate r_o increased with increasing c, and more so for larger r. The form of the dependence of r_o on c was more saturating for larger r. The output rate of the FR neuron with identical input parameters, but using the MIP model as excitatory input, is

shown in Figure 3D. We observe a distinct difference with the response to the SIP input, particularly for small input correlations. Here, for small c, an increase of c leads to a large increase of r_o due to the large N. A consecutive decrease of r_o for larger c occurred for small r only. Indeed, for $r = 50, 90$ spikes per second, the inter-cluster interval did not become small compared to the membrane time constant.

After having explored the effects of each of the three input parameters, we now consider how modifications of the FR neuron and, more precisely, of the membrane time constant τ, the threshold θ of the activation function, and the form of the activation function could affect these results. With regard to τ, note that the output rate of the FR neuron with the SIP model (see equation 3.6) depends only on the product $r\tau$. Thus, an increase (decrease) of the time constant has the same effect as the proportional increase (decrease) of the input rate. This is the case for the density function of any shot noise with exponential kernel (Gilbert & Pollak, 1960). Taking into consideration that the membrane potential of the FR neuron response (for both the SIP and the MIP models) can be decomposed into a sum of several elementary shot noise processes with different amplitudes and rates (see appendix B), it can be concluded that the equivalence of τ and r is valid for all input parameters of both input models. An analogous but somewhat weaker statement can be made concerning the threshold θ of the activation function. The output rate of the neuron depends only on the quotient θ/N (see equation 3.6). This is the case for the approximated response to both the SIP and the MIP models (see appendix B). Thus, as long as the approximation is good, the effect of an increase of θ is equivalent to the proportional decrease of N.

Finally, we turn to the effects of the form of the activation function. For an arbitrary function, it would be necessary to know the entire density function of the potential to be able to derive the mean output rate of the FR neuron. The piecewise definition of the density function, however, makes it difficult to derive an approximation of the output rate. Nevertheless, our method would still be applicable, and an approximation of the neuronal rate could be derived, if the input clusters had a low rate. Indeed, in this case, the entire density function is well approximated by the first few segments. Note that if the activation function was linear, the mean output rate of the FR neuron would not be sensitive to any aspect of the input statistics other than the mean input rate, because the mean output of a linear system is determined by its mean input only. A nonlinear activation function is thus a prerequisite for the sensitivity of the neuron to input correlations and, *a fortiori*, to higher-order statistics. In turn, any sufficiently nonlinear activation function will result in different mean responses of the FR neuron to both input models. Indeed, the response potential densities to both the SIP and MIP model are different, and the mean output rate will typically be different.

3.2 Response of the Integrate-and-Fire Neuron. In order to compare the effects of different input ensemble statistics under more realistic condi-

tions, we simulated a conductance-based leaky IF neuron (Tuckwell, 1988; Koch, 1999). Its membrane potential was (on average) depolarized with respect to the resting state, and it fluctuated. Its input conductance was also increased, similarly to what is typically observed *in vivo* (Paré, Shink, Gaudreau, Destexhe, & Lang, 1998).

The essential difference to the membrane potential dynamics of the FR neuron is that synapses here were modeled not as current pulses but as transient membrane conductance changes. The subthreshold membrane potential of the IF neuron was described by

$$C\frac{d}{dt}U(t) = \frac{1}{R}[U_r - U(t)] + G_e(t)[U_e - U(t)] + G_i(t)[U_i - U(t)].$$

U_r is the resting membrane potential. $G_e(t)$ and $G_i(t)$ are the excitatory and inhibitory synaptic conductances, and U_e and U_i are the excitatory and inhibitory synaptic reversal potentials, respectively. We use $g_e(t)$ and $g_i(t)$ to denote the conductance changes elicited by a single excitatory or inhibitory presynaptic spike. Both excitatory and inhibitory conductance changes were modeled by an α-function (Koch, 1999; Rotter & Diesmann, 1999),

$$g_e(t) = \overline{g}_e ate^{1-at}H(t), \qquad G_e(t) = \sum_k g_e(t - t_k^e),$$
$$g_i(t) = \overline{g}_i ate^{1-at}H(t), \qquad G_i(t) = \sum_k g_i(t - t_k^i),$$

where $\overline{g}_e$ ($\overline{g}_i$) is the peak excitatory (inhibitory) conductance change, and $1/a$ is the time constant of the conductance change. Both types of synapses had the same time constant. The times t_k^e and t_k^i represent the occurrences of excitatory and inhibitory input spikes, respectively. The voltage-dependent conductances responsible for the action potential generation were not included in the model. Instead, when the membrane potential reached a threshold U_θ, an action potential was generated and the membrane potential was clamped to a reset value U_{reset} for a period t_{refr}. In addition, all synaptic currents were shunted. This latter mechanism modeled the refractory period.

The various model parameter values were chosen to be in line with the experimental literature (McCormick, Connors, Lighthall, & Prince, 1985): $C = 500$ pF, $R = 30$ MΩ, $U_r = -70$ mV, $U_\theta = -50$ mV, $U_{\text{reset}} = -60$ mV (Troyer & Miller, 1997), and $t_{\text{refr}} = 2$ ms. The excitatory synapses modeled fast glutamatergic (AMPA) synapses, and the inhibitory synapses modeled fast GABAergic (GABA_A) synapses. We set $U_e = 0$ mV and $U_i = -70$ mV (Koch, 1999). The time constant of the synaptic conductance changes was $1/a = 1$ ms, and the peak conductances were $\overline{g}_e = 1$ nS and $\overline{g}_i = 3.4$ nS, respectively.

3.2.1 Membrane Potential Response. A depolarized membrane potential was obtained by bombarding the neuron with Poisson spike trains. We used independent excitatory and inhibitory spike trains whose rates were

adjusted such that the membrane potential fluctuated around a mean value of −54.3 mV (Léger, Stern, Aertsen, & Heck, 2002). We used an excitatory rate of 9000 spikes per second and an inhibitory rate of 5500 spikes per second, which is equivalent to 9000 independent individual excitatory inputs and 5500 independent individual inhibitory inputs, both with a rate of 1 spike per second. We refer to this input as background input. The membrane potential fluctuated with a standard deviation of 1.5 mV, and the model neuron fired with a rate of 1 spike per second under these conditions. The excitatory postsynaptic potential (EPSP) or inhibitory postsynaptic potential (IPSP) produced by an additional excitatory (inhibitory) input spike had, on average, an amplitude of 0.16 mV (−0.15 mV). This is in accordance with Matsumura, Chen, Sawaguchi, Kubota, & Fetz (1996), who found that EPSPs and IPSPs recorded intracellularly *in vivo* had similar amplitudes and time courses.

We let two additional populations of excitatory and inhibitory inputs impinge on the neuron. Both populations had the same size, and the individual excitatory and inhibitory discharge rates were identical, as with the FR neuron. The excitatory spike trains were correlated, with parameters represented by either the SIP or the MIP model; the inhibitory inputs were always independent. Figure 4A shows a 500 ms realization of the excitatory and inhibitory population activity (bottom), with $N = 100$ and $r = 20$ spikes per second. Both the input and the IF neuron were simulated with a time step of 0.1 ms. In the figure, the number of excitatory input spikes per time step is plotted as a positive integer and the number of inhibitory input spikes per time step as a negative integer. The SIP model was used for the excitatory population, and the correlation coefficient was $c = 0.1$. Note that the background synaptic input is not shown. The membrane potential response of the IF neuron is plotted in the upper part of the figure. It fluctuated randomly, characterized by occasional fast depolarizations leading to an output spike. These were mostly caused by spike clusters involving the whole correlated excitatory population. Note that the second spike in Figure 4A was due to the background of independent synaptic input. The same input parameters were used for Figure 4B, but here the MIP model replaced the SIP model. The excitatory input activity consisted of a large number of clusters of smaller size; the output spikes resulted from the summation of several input clusters. This summation mechanism was rendered stochastic by the background fluctuations of the membrane potential. Due to the reduced size of the input clusters, the depolarization preceding a response spike was slower than with the SIP model.

In Figure 4C, we used the SIP model but increased the pairwise correlation coefficient to 0.4. As a consequence, the rate of occurrence of the input clusters increased, accompanied by a corresponding increase of the output rate. Figure 4D shows the response of the neuron to the MIP model, with $c = 0.4$. The size of the clusters increased compared to $c = 0.1$ (see Figure 4B), but their rate of occurrence decreased, as already explained in section 3.1.

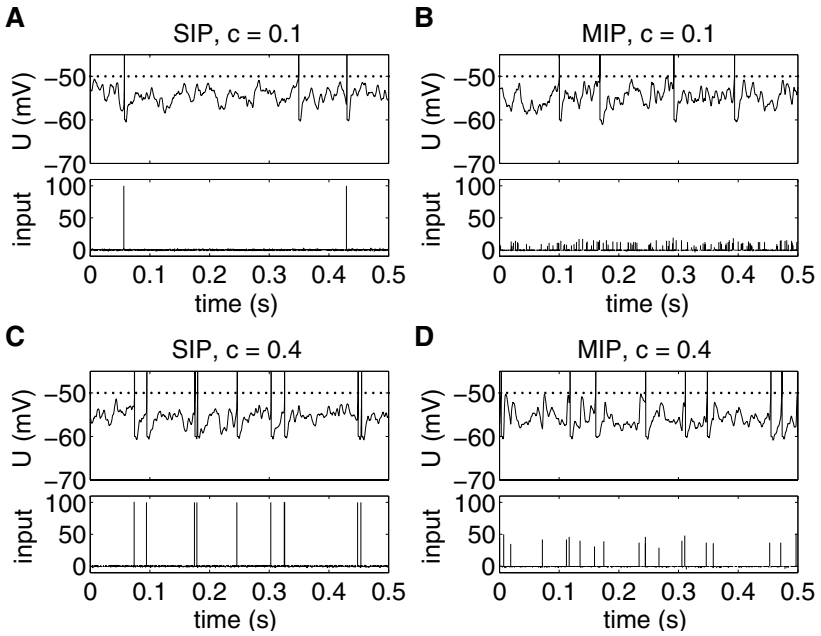

Figure 4: Time course of the membrane potential of the leaky integrate-and-fire (IF) neuron (top) and the corresponding input (bottom), with the excitation generated by either the SIP or the MIP model. (A) The excitation was generated according to the SIP model, with a pairwise correlation coefficient of 0.1; the inhibition was a population of independent Poisson processes. The input population size ($N = 100$) and individual firing rate ($r = 20$ spikes per second) were the same for the excitation and the inhibition. The number of excitatory (inhibitory) input spikes per bin (size 0.1 ms) is plotted as a positive (negative) number in the lower panel. Note that the additional independent background inputs that kept the membrane potential in a depolarized state (see text) are not shown. The dotted line in the upper panel indicates the firing threshold. (B) The excitation was generated according to the MIP model. The pairwise correlation and other input parameters were identical to *A*. (C) The excitation was generated according to the SIP model, with an excitatory input pairwise correlation coefficient of 0.4. Other parameters as in *A*. (D) The excitation was generated according to the MIP model. The pairwise correlation and other input parameters were identical to *C*.

The output rate was larger than with $c = 0.1$. However, the clusters were still not large enough to reliably elicit an output spike individually.

3.2.2 Mean Response Rate. Similarly to the FR neuron, we compared the response of the IF neuron for the two different input models SIP and

MIP by studying the dependence of the output firing rate on the pairwise correlation of the excitatory input. In addition, we systematically varied N and r. Figure 5A shows the output rate r_o of the IF neuron to SIP input as a function of c, for a fixed input rate $r = 20$ spikes per second, and for different input population sizes $N = 20, 40, 100, 1000$. The output rate slowly increased with the input correlation coefficient. For population sizes beyond 100, the output rate r_o did not increase any further. This behavior was caused by the membrane potential resetting of the IF neuron. Evidently, if the input population size is large enough that the depolarizations induced by an input cluster reach the threshold, a further increase of N has no impact on the output rate because the rate of occurrence of the input clusters does not depend on N. In that case, the mean output rate r_o of the IF neuron can thus be approximated by (see Murthy & Fetz, 1994)

$$r_o = \rho(1 - \tau_{\text{refr}} r_o), \tag{3.7}$$

where ρ is the rate of input clusters. For the SIP model, we have $\rho = rc$. This approximation is plotted as a thick gray line in Figure 5A and expresses that the output rate r_o is equal to the rate of spike clusters ρ, subtracting the clusters arriving while the neuron is refractory. Of course, the approximation is not valid if output spikes are (also) caused by the background bombardment of non-synchronized excitatory spikes (as is the case for $c = 0$, for instance).

Figure 5B shows the response of the IF neuron as a function of c but with the MIP model for the excitation and for $r = 20$ spikes per second and $N = 20, 40, 100, 300, 500, 1000$. For small values of c, the dependence of the output rate on c was far more strongly modulated than with the SIP model. For $N = 1000$, for instance, a small c generated a very large output firing rate, much larger than with the SIP model. Only for very small populations ($N = 20$) was the output rate smaller than with the SIP model, over the whole range of c (see Figure 5A, inset). For large N, as for the FR neuron, the dependence of r_o on c was non-monotonic. The initial increase of r_o with c was caused by the integration of increasingly large input clusters. However, when the clusters were large enough that the occurrence of a single input cluster reliably triggered an output spike, a further increase of the input correlation was detrimental to the output firing rate. Indeed, a further increase of c, resulting in even larger input clusters, causes r_o to decrease, because the occurrence rate of clusters decreases with increasing c. For these larger values of c, the mean output rate r_o of the IF neuron can again be approximated by equation 3.7. We assume that the stochastic nature of the spike cluster size does not play a role and replace each cluster by one of average amplitude. The rate of the mean amplitude clusters is r/c. The approximation given by equation 3.7, with $\rho = r/c$, is represented as a thick gray line in Figure 5B. The amplitude of the mean input spike cluster is proportional to N, and the range of validity of the approximation is larger

for large values of N. Note that for larger values of r_o, the approximation slightly overestimated the output rate. This is due to the finite rise time of the conductances used to model the synapses, which allowed synchronized clusters to impinge on the cell during the depolarization caused by a first cluster. Such an event happened more frequently at higher rates.

Figure 5C shows the mean output rate of the IF neuron with the SIP model, for $N = 500$, and $r = 10, 20, 50, 90$ spikes per second. N was large enough so that each input cluster elicited an output spike. The relation between r_o and c depended on r, because the rate of occurrence of the input clusters is proportional to r. The mean output rate was approximated by equation 3.7, with $\rho = rc$ (thick gray lines). Again, note that the approximation is more precise for small values of r_o. We replaced the α-function conductance with a conductance pulse and repeated these simulations. In that case, the (small) discrepancy between the simulated output rate and the approximation, observed for larger values of r_o, disappeared completely (data not shown).

The response to exactly the same input parameters, but with the MIP model instead of the SIP model, is shown in Figure 5D. As N was large, a non-monotonic dependence of r_o on c could be observed. This was the case for all r. The approximation of the mean output rate r_o (see equation 3.7, $\rho = r/c$) is plotted as thick gray lines. For the different input rates r, the left bound of the range of the approximated output rate was chosen as the value of c producing the maximal output rate in the numerical simulations. The approximation gave better results for small values of output rates, as explained above. For large r (50, 90 spikes per second), two local maxima appeared in the simulation results for the dependence between r_o and c. For the smaller value of c, the interaction structure was thus (locally) optimal with regard to the generation of output spikes, so that both an increase and a decrease of c caused a decrease of r_o. To first approximation, we can make the same assumption here as for the response of the FR neuron and explain this effect in terms of the mean cluster. The mean cluster generated by the MIP model, for a value of c producing the locally maximal output rate, was not big enough to depolarize the membrane potential up to the spiking threshold alone and thus needed support from other inputs. An efficient arrangement consists of pairs of clusters whose sizes were such that within the integration time of the membrane, they jointly cause a depolarization that can just bring the neuron to fire a spike. A pair of larger clusters would result in the same effect, but it would occur less frequently, as the mean cluster rate is inversely related to its mean size. Note that the positions of both peaks are shifted to higher values of c for increasing input rate r. This is because not only excitation but also inhibition increases with r, necessitating larger clusters to reach the threshold. Interestingly, this can lead to a non-monotonic dependence of r_o on r. For c around 0.35, for instance, an increase of the input rate from 50 to 90 spikes per second resulted in a decreased output rate.

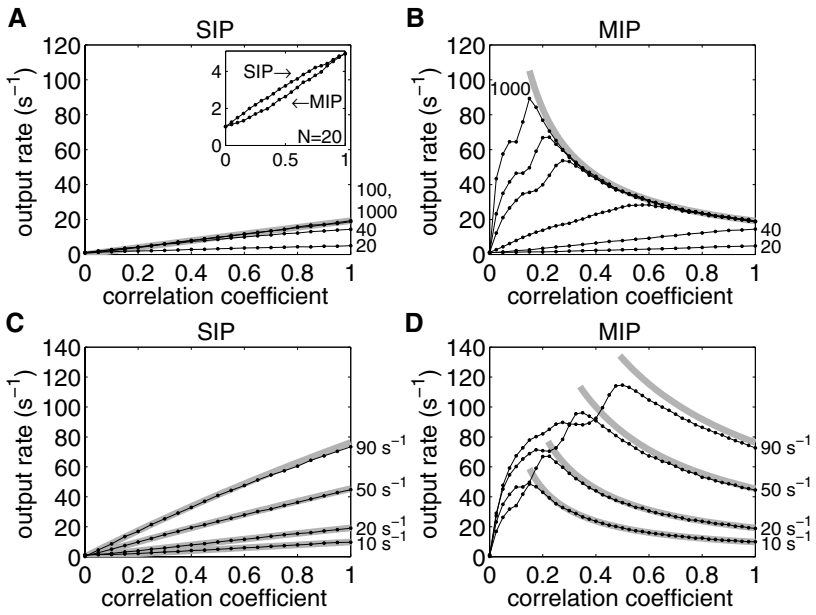

Figure 5: Mean output rate of the leaky integrate-and-fire (IF) neuron as a function of the pairwise correlation coefficient of the excitatory input, for the two different input ensemble statistics. Thick gray lines represent an analytical approximation of the output firing rate under the assumption of large spike clusters in the input (see text for details). (A) The excitation was generated according to the SIP model; the inhibition was a set of independent Poisson processes. Excitatory and inhibitory population size and rate were identical. The output rate is shown for different input population sizes ($N = 20$, 40, 100, 1000) and constant individual input rate ($r = 20$ spikes per second). The output rate for $N = 100$ and $N = 1000$ produced undistinguishable curves. The inset compares the response of the IF neuron for the SIP and the MIP input model as excitation, for $N = 20$ and $r = 20$ spikes per second. It shows that for small population sizes, the output rate with the SIP model was larger over the whole range of c. (B) The excitation was generated according to the MIP model. The output rate is shown for different input population sizes ($N = 20$, 40, 100, 300, 500, 1000) and a fixed input rate ($r = 20$ spikes per second). (C) Same input setting as in A, for different individual input rates ($r = 10$, 20, 50, 90 spikes per second) and a fixed population size ($N = 500$). (D) The excitation was generated according to the MIP model. All input parameters as in C. Again, note that for $c = 0$ and $c = 1$ the SIP and the MIP model coincide.

The input scenarios discussed thus far were composed of equal proportions of excitation and inhibition. The ratio of excitation and inhibition received by a cortical neuron *in vivo*, however, can only be roughly estimated. Anatomical data suggest that excitation amounts to more than four times the inhibition (Braitenberg & Schüz, 1998). On the other hand, it has been argued on the basis of the irregularity of the discharge of cortical neurons that they operate with equal proportions of excitation and inhibition (van Vreeswijk & Sompolinsky, 1996; Shadlen & Newsome, 1998). We define the balance of the input,

$$b = \frac{N_i r_i}{N_e r_e},$$

where N_e (N_i) is the excitatory (inhibitory) input population size and r_e (r_i) the firing rate of individual excitatory (inhibitory) input lines. We varied the input balance of the IF neuron by changing the amount of inhibition (the product $N_i r_i$). Note that the same variation of b could be obtained by changing either N_e or r_e, not necessarily leading to exactly the same effects. Figure 6A shows the mean output rate of the IF neuron as a function of the excitatory pairwise correlation, for different levels of inhibition, using the SIP model for the excitatory input. The excitation was composed of $N_e = 300$ and $r_e = 20$ spikes per second. The inhibition was $N_i r_i = 0$, 1200, 3000, 6000, or 9000 spikes per second, corresponding to $b = 0$, 0.2, 0.5, 1, 1.5. For low levels of inhibition ($b = 0$, 0.2, 0.5), the output firing rate for weak pairwise correlations in the input was much larger than for the balanced input. For these values of b, an increase of c caused a decrease of the output rate. The occurrence of excitatory clusters of size N_e induced large depolarizations—larger than actually necessary to reach the spiking threshold. The excess excitatory spikes hence did not contribute to generating output spikes, which had a detrimental effect on the output rate. Observe that for $b = 0.5$, r_o decreased down to a value of 10 spikes per second at $c = 0.45$ and increased up to about 20 spikes per second at $c = 1$. Thus, the initial decrease of r_o, caused by spikes participating in the (too) large synchronization clusters, could be partially compensated for by the increased cluster rate. Using more inhibition than excitation ($b = 1.5$), no output spikes were produced for independent inputs. Due to the hyperpolarized membrane potential, the fluctuations of the potential were not large enough to induce spontaneous spiking. Nevertheless, an increase of the input correlation and the associated occurrence of synchronized clusters brought the neuron to fire, with an output rate again tending to the maximal rate of 20 spikes per second for $c = 1$. This is shown by the overlap with the thick gray line, representing the approximation expressed by equation 3.7 (with $\rho = rc$).

The response of the IF neuron to the same input parameters, but with the MIP model instead of the SIP model for the excitatory input, is shown in Figure 6B. We again observe considerable differences with the response

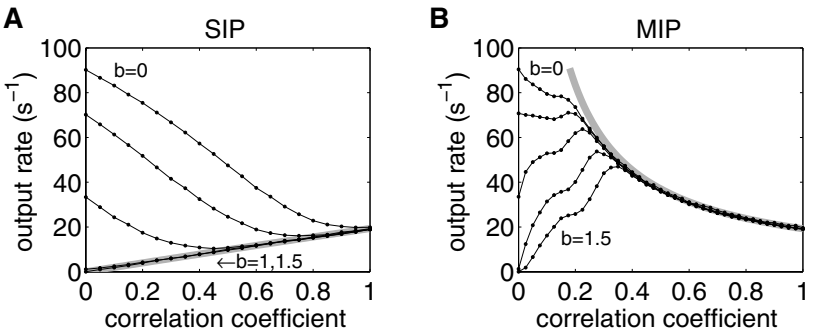

Figure 6: Mean output rate of the leaky integrate-and-fire (IF) neuron as a function of the pairwise correlation coefficient of the excitatory input, for the two different input ensemble statistics, with different ratios of inhibition to excitation. Thick gray lines represent an analytical approximation of the output firing rate, assuming that output spikes are caused only by large spike clusters in the input. (A) The excitation was generated according to the SIP model. The excitatory population size was $N_e = 300$, and the excitatory individual firing rate was $r_e = 20$ spikes per second. The product of the inhibitory population size and rate was $N_i r_i = 0, 1200, 3000, 6000, 9000$, corresponding to an input balance (see text) of $b = 0, 0.2, 0.5, 1, 1.5$. The response of the IF neuron for $b = 1.5$ and $b = 1$ differed only for very low excitatory input correlations. (B) The excitation was generated according to the MIP model. All input parameters were identical to *A*.

to the SIP input, particularly for small input correlations. At small values of c, a small increment induced a large increase of r_o for $b = 1$ and 1.5. For $b = 0.2$, a small increase of c had little influence on r_o, and for $b = 0$, r_o decreased with c. Small values of c generated small synchronized clusters that could drive the output rate up or down, depending on the net excitation level. This is because for high inhibition levels, the membrane potential fluctuates strongly, and an increase of excitatory input synchrony results in an even higher variance of the membrane potential, leading to more frequent threshold crossings. By contrast, if the excitation level is high, the synaptic input, on average, tends to depolarize the neuron above threshold (see Shadlen & Newsome, 1998). In that case, the summation of rapidly occurring excitatory spikes is efficient, and synchrony does not greatly accelerate the depolarization of the membrane potential to threshold. For $b = 0.2$, r_o was initially insensitive to changes in c, because the loss of spikes in the synchronized clusters was exactly compensated by the greater efficacy of synchronous input. The degree of input balance at which this effect occurs depends on the input parameters N and r. For larger c, as N was large, the effect of synchrony was detrimental for all b values. As the output spikes were then exclusively caused by clusters of synchronous

input spikes, the mean response rate was well described by the approximation expressed by equation 3.7 (with $\rho = r/c$), plotted as a thick gray line in Figure 6B.

The interaction structure of the input can thus have a dramatic influence on the output firing rate. A striking example is given by the response of the IF neuron for $b = 0.5$. With the interaction structure of the SIP type, an increase of c from 0 provoked a decrease of the output firing rate, but with the MIP model, for the same input balance level, the same increase of correlation induced an increase of the output rate.

4 Discussion

Individual firing rates and pairwise correlations of a population of neurons do not determine the ensemble uniquely. We showed that neurons can be very sensitive to the details of the interaction structure of their input ensembles. Thus, it is difficult to draw any definitive conclusions about the effect of particular input parameters (like pairwise correlation) on a neuron's output rate, as long as physiological input ensembles are not characterized in a more complete manner, in particular, by specifying their higher-order correlation structure.

4.1 Input Ensemble Statistics. In model studies, it is often assumed that the total input or the membrane potential can be represented by a process with a gaussian probability density function (Tuckwell, 1988; Feng & Brown, 2000; Svirskis & Rinzel, 2000). Doing so has the advantage that the statistical properties of the model can be constrained easily. Nevertheless, as the third and higher cumulants are forced to be zero, this model is obviously not suited to study the impact of the full ensemble statistics. As we have shown in this work, it is crucial to take all moments of the input ensemble into account.

Several studies have tackled the impact of correlated spike trains on the output of neuron models. Shadlen and Newsome (1998) and Salinas and Sejnowski (2000) generated correlated spike trains by simulating neurons with partial common input. Two sets of inputs were randomly drawn from a finite pool, resulting in a certain fraction of the inputs being used for both neurons. This introduces a correlation in the output spike trains of the two neurons. Such spike trains have broader cross-correlograms, which is more realistic than the exact synchrony used in this study. However, the higher-order interactions in such ensembles of spike trains were not considered. Another drawback is that the ensembles were not defined analytically. Destexhe and Paré (1999) used correlated synaptic input to reproduce the neuronal properties observed *in vivo*. They used Poisson processes as inputs and introduced stochastic dependence by drawing a smaller number of input processes than there were synapses (similarly to Salinas & Sejnowski, 2000), a single Poisson process being used as input to several synapses.

Again, the relation between the pairwise correlation and the higher-order correlation structure was not stated explicitly.

Statistically, the interaction structure of an input ensemble has a large number of degrees of freedom. We picked two extreme situations. In the SIP model, all of the doublets of spikes on any pair of spike trains occur simultaneously, resulting in spike clusters synchronized over the whole population. In the MIP model, the cluster size is a stochastic variable with a mean increasing linearly with the pairwise correlation. To realize a pairwise correlation coefficient identical to the SIP model, the average cluster rate must be higher than in the SIP model. Some studies used an input ensemble related to the MIP model (Murthy & Fetz, 1994; Bernander, Koch, & Usher, 1994) in order to investigate the effects of input synchrony. Their input ensemble differed from ours in that the rate of occurrence of spike clusters was held constant. As a consequence, they parameterized their ensemble in terms of the absolute synchrony (the size of spike clusters), and not in terms of the correlation coefficient. Interestingly, Bernander et al. (1994) also introduced a temporal jitter of the synchronization and showed that the precision of the spike correlation can strongly modulate the output firing rate, depending on the values of the input parameters.

The issue of the ensemble statistics was specifically tackled by Bohte et al. (2000), who studied an input distribution with maximal entropy. Assuming homogeneous rates and homogeneous pairwise correlations, they derived a maximally flat distribution of input clusters. The size of an input cluster was defined as the number of neurons spiking within a single time bin. They showed that under the assumption of maximal entropy, spike clusters involving a large number of neurons already exist for a small pairwise correlation.

The SIP and MIP models were chosen because they represent two extreme cases of input ensembles. The question arises of how similar they are to the inputs that a real cortical neuron receives. To date, this question remains largely unanswered. Let us mention two lines of research that could help solve this problem. The first is the massively parallel recording of multiple single cell activities *in vivo* (Nicolelis, 1998). Statistical methods suited to the analysis of the corresponding data are beginning to be available (Gerstein & Aertsen, 1985; Martignon et al., 1995, 2000; Gütig et al., 2002). Nevertheless, the pool of neurons forming the actual presynaptic input ensemble to a single cortical neuron cannot be inferred from such studies. Therefore, a second source of answers could come from the detailed investigation of membrane potential fluctuations gained from intracellular recordings *in vivo* (Borg-Graham, Monier, & Frégnac, 1998; Azouz & Gray, 1999; Léger, Stern, Aertsen, & Heck, 2002). Analysis of membrane potential fluctuations or their time courses, possibly combined with simultaneous recordings from neighboring cells, could help to shed light on the interaction structure of the input ensembles seen by cortical neurons.

4.2 Dependence of Response on Input Ensemble Statistics. We used the SIP and MIP models of spike train ensembles to describe the excitatory input into neurons. The inhibitory inputs were assumed independent throughout this study. With the SIP model and for a fixed pairwise input correlation, an increase of the input population size induced only a limited increase of the output rate for two very different neuron models (see Figures 3A and 5A). This was true at all input rates and over the entire range of input correlations. Interestingly, this was the case not only for the IF neuron but also for the FR neuron, whose membrane potential did not undergo any reset following a threshold crossing. Probing the model neurons with an interaction structure generated by the MIP model, we observed that for any fixed pairwise correlation in the input, the range of output rates obtained by varying the size of the input ensemble was much larger than with the SIP model (see Figures 3B and 5B). For small input correlations and in contrast to what happened with an interaction structure of the SIP type, the output rate increased steadily with the size of the input ensemble and could thus attain much larger values.

The most striking difference between the response to both interaction structures was observed for large input populations. By large, we mean that an input spike cluster involving the whole population elicits a membrane depolarization that reaches the firing threshold. With the SIP model, the rate of spike clusters was proportional to both the individual input rate and the pairwise correlation. For a large input population, the output rate of the IF neuron was thus approximately linearly related to these two input parameters (see Figure 5C). By contrast, with input statistics of the MIP type, the dependence of the IF response on the input firing rate of a large input ensemble could be non-monotonic (see Figure 5D).

Note that for the FR neuron, the variance of the membrane potential was the same with the SIP or the MIP input model. Indeed, the autocovariance function (and thereby the variance) of a linear system's output is entirely determined by the autocovariance function of its input (Papoulis, 1991). As the autocovariance of the summed input ensemble is given by the sum of the autocovariances and cross-covariances of the individual spike trains (both of which were identical for the SIP and the MIP input models), the autocovariance of the membrane potential is identical for both input ensembles. Thus, the size of the fluctuations, as measured by the variance of the membrane potential, does not alone explain the output rate response, as shown by the very different response of the FR neuron to both input ensembles (see Figure 3). This also implies that the assumption of a gaussian distribution of the membrane potential, which requires knowing only the first and second moments of the potential, may fail to predict the mean response rate. Moreover, it can be easily shown that the variance of the membrane potential increases (monotonically) with the input pairwise correlation c (see appendix B for the complete expression of the variance of the membrane potential). Thus, despite an increasing vari-

ance of the membrane potential, the response rate can decrease (see Figures 3B and 3D), depending on the higher-order interactions of the input ensemble.

Many of the neuronal response properties investigated here were similar for both the FR and the IF neuron. The differences could originate from either the postspike reset mechanism built into the IF neuron or from the use of conductances to model the synapses. Tiesinga, José, and Sejnowski (2000) studied the differences in the neuronal response to an uncorrelated input ensemble when using currents or conductances to model synapses. In the case of the MIP model, we have previously shown that the mean output of a continuous FR neuron with reversal potentials can be in very good correspondence to the output rate observed in an otherwise identical neuron that included a membrane potential reset mechanism (Kuhn, Rotter, & Aertsen, 2002).

Hence, depending on the higher-order statistics of the input ensemble, input parameters can have very different effects on the neuron's output rate. We studied the effects of pairwise correlation in the excitatory population across its entire range from 0 to 1. However, in experimental studies, the correlation coefficient is rarely found to be larger than 0.1 to 0.2 (Aertsen & Gerstein, 1985; Das & Gilbert, 1999; Eggermont & Smith, 1995; Nelson, Salin, Munk, Arzi, & Bullier, 1992). Considering this range of input correlations, it appears that the two different realizations of input correlations considered here impose different constraints on the way the neuronal response can be modulated. If the activity of a presynaptic network is characterized by the synchronization of large pools of neurons, the neuronal output is approximately linearly modulated by the input rate. By contrast, if the population activity of the presynaptic network is composed of small, distributed clusters, the size of the input population constitutes an ideal parameter to modulate the output firing rate of the postsynaptic neuron over a large range. The latter case would thereby suggest an operation mode based on the dynamic recruitment of input lines.

4.3 Balance of Excitation and Inhibition. We changed the mean ratio of inhibition to excitation of the input (the input balance) and observed that the effects of pairwise correlation in the excitatory population on the output rate could be reversed. With the SIP model as excitatory input structure, the monotonic increase of the output rate as a function of the correlation, observed for equal proportions of excitation and inhibition, could change into a monotonically decreasing relation (see Figure 6A). Such modulation of the relative effect of synchrony by the net excitatory level was also observed with the MIP model as interaction structure for low values of the input correlation coefficient (see Figure 6B). This detrimental effect of input synchrony on the postsynaptic firing, at high levels of (net) excitation, has already been reported (Murthy & Fetz, 1994), albeit with a different input ensemble (see above).

Stroeve and Gielen (2001) used an input population identical to the SIP model and reported that the pairwise correlation of excitation affects the postsynaptic firing rate only if the inhibitory firing rate is sufficiently high. It must be pointed out that this statement follows from their particular choice of input parameters. They used a small input size ($N = 120$), which was effectively smaller compared to the input used here because the membrane potential of their model neuron was not in a depolarized state. As shown in this study, the effects of input correlation depend strongly on the size of the population. More important, their input parameters were such that a compensation effect, similar to what was described for Figure 6B ($b = 0.2, c < 0.2$), was in effect. This is clearly demonstrated by the irregularity of inter-spike intervals (Stroeve & Gielen, 2001) that increased with the input correlation. This shows that the neuron's firing was increasingly caused by large, randomly occurring spike clusters. As such input clusters induced membrane depolarizations beyond the firing threshold, the corresponding "loss of spikes" had to be compensated for by the increased efficacy of synchrony.

Hence, as demonstrated in Figure 6B for low input correlation, it is appropriate to consider the net excitation level as a powerful means of modulating the effects of input correlation. This possibility was mentioned earlier by Salinas and Sejnowski (2000). Finally, we would like to stress that both input and output investigated here were stationary and that an important and obvious step toward more realistic conditions would be to study the impact of nonstationary input ensemble statistics.

Appendix A

In this appendix, we derive the cross-correlation function and count correlation coefficient for pairs of spike trains generated by either the SIP or the MIP model. Consider a homogeneous Poisson point process $x(t)$ with rate $\mathrm{E}[x(t)] = \lambda$. The autocorrelation $R_{xx}(\Delta t)$ of this process is (Papoulis, 1991)

$$R_{xx}(\Delta t) = \mathrm{E}[x(t)x(t + \Delta t)] = \lambda\delta(\Delta t) + \lambda^2.$$

For two independent Poisson point processes $x(t)$ and $y(t)$ with rates λ and μ, respectively, the cross-correlation function $R_{xy}(\Delta t)$ is

$$R_{xy}(\Delta t) = \mathrm{E}[x(t)y(t + \Delta t)] = \lambda\mu.$$

We now consider dependent processes. Let $v(t)$ and $w(t)$ be defined as

$$v(t) = x(t) + z(t)$$
$$w(t) = y(t) + z(t),$$

where $x(t)$, $y(t)$, and $z(t)$ are independent homogeneous Poisson processes with rate λ, μ, and ν, respectively. The cross-correlation function of $v(t)$ and

$w(t)$ is

$$\begin{aligned} R_{vw}(\Delta t) &= R_{xy}(\Delta t) + R_{xz}(\Delta t) + R_{yz}(\Delta t) + R_{zz}(\Delta t) \\ &= \nu\delta(\Delta t) + \nu^2 + \lambda\nu + \mu\nu + \lambda\mu \\ &= \nu\delta(\Delta t) + (\nu + \lambda)(\nu + \mu). \end{aligned}$$

The count correlation coefficient for the two point processes $v(t)$ and $w(t)$ with respect to a fixed observation interval of duration T is defined in terms of the stochastic variables V and W giving the respective numbers of points encountered during the observation interval:

$$c_{VW} = \frac{\mathrm{cov}(V, W)}{\sqrt{\mathrm{var}(V)\mathrm{var}(W)}}.$$

For arbitrary point processes, the count correlation coefficient depends in general on the observation interval. For the two dependent Poisson processes $v(t)$ and $w(t)$ considered above, we have in particular

$$\begin{aligned} \mathrm{var}(V) &= \mathrm{var}(X) + \mathrm{var}(Z) \\ \mathrm{var}(W) &= \mathrm{var}(Y) + \mathrm{var}(Z) \\ \mathrm{cov}(V, W) &= \mathrm{var}(Z), \end{aligned}$$

with X, Y, and Z the stochastic variables giving the respective numbers of points in the processes $x(t)$, $y(t)$, and $z(t)$, in the interval considered. For an observation interval of duration T, we have

$$\mathrm{var}(X) = \lambda T, \quad \mathrm{var}(Y) = \mu T, \quad \mathrm{var}(Z) = \nu T,$$

and thus obtain

$$c_{VW} = \frac{\nu}{\sqrt{(\nu + \lambda)(\nu + \mu)}}.$$

Note that this is independent of the observation length T. Thus, we may also simply use the term "pairwise correlation coefficient" for "count correlation coefficient." Normalizing the cross-correlation function of the two processes by the geometric mean of their respective rates, we obtain an expression of the cross-correlation as a function of the count correlation coefficient,

$$\frac{R_{vw}(\Delta t)}{\sqrt{(\nu + \lambda)(\nu + \mu)}} = c_{VW}\delta(\Delta t) + \sqrt{(\nu + \lambda)(\nu + \mu)}.$$

The count correlation coefficient thus corresponds to the net integral over the central peak in the (normalized) cross-correlation function.

The general case represented by $v(t)$ and $w(t)$ is now readily applied to our two models of spike train ensembles. For the SIP model, we have $\nu = \alpha$

and $\lambda = \mu = \beta$. Hence, the cross-correlation function and count correlation coefficient between any two spike trains are

$$R(\Delta t) = \alpha\delta(\Delta t) + (\alpha + \beta)^2,$$
$$c = \frac{\alpha}{\alpha + \beta}.$$

For the MIP model, it holds that the rate of coincident spikes in any pair of spike trains is $\nu = \gamma\epsilon^2$ and $\lambda = \mu = \gamma\epsilon - \gamma\epsilon^2$. The cross-correlation function and count correlation coefficient thus are

$$R(\Delta t) = \gamma\epsilon^2\delta(\Delta t) + (\gamma\epsilon)^2,$$
$$c = \epsilon.$$

Appendix B

In this appendix, we develop an analytical approximation of the response of the FR neuron to the two models of spike train ensembles (SIP and MIP). The FR neuron was described above (see equations 3.1 through 3.3). The corresponding synaptic input current is described by a stationary stochastic process, and we are interested in the stationary output rate of the neuron. The knowledge of the stationary membrane potential distribution is sufficient to derive the mean output rate for this particular neuron model (see equation 3.5). If we use linear synapses and Poisson-driven synaptic events, the membrane potential is a shot noise. For pulse-like synaptic currents, the membrane realizes a first-order low-pass filter with time constant $\tau = RC$ (see equation 3.4).

Gilbert and Pollak (1960) derived an integral equation for the shot noise distribution and solved it for several particular choices of the filter. For the filter $h(t)$ defined in equation 3.4, with $A = 1$ and $\tau = 1$, the shot noise $S(t)$ with underlying rate λ has an amplitude distribution with density $P(S)$ given by

$$P(S) = dS^{\lambda-1} \qquad \text{for } 0 \le S < 1.$$

For larger values of S, $P(S)$ is found by recursion from the integral equation,

$$P(S) = S^{\lambda-1}\left[d - \lambda\int_1^S P(x-1)x^{-\lambda}\,dx\right].$$

The constant d is given by

$$d = \frac{e^{-\lambda g}}{\Gamma(\lambda)},$$

where $g = -\int_0^\infty e^{-t} \log t \, dt$ is Euler's constant and $\Gamma(z) = \int_0^\infty t^{z-1} e^{-t} \, dt$ is the gamma function. Thus, the analytic expression of $P(S)$ changes at integer values of S. For τ arbitrary, the density is easily shown to be

$$P_\star(S) = \begin{cases} DS^{\lambda\tau - 1} & \text{for } 0 \le S < 1 \\ DS^{\lambda\tau - 1}\phi(\lambda\tau, S) & \text{for } 1 \le S < 2 \end{cases} \tag{B.1}$$

where

$$\phi(\lambda\tau, S) = 1 - \left[\left(\frac{1}{S-1} \right)^{-\lambda\tau} F(\lambda\tau, \lambda\tau, 1 + \lambda\tau; 1 - S) \right]$$

and F is the hypergeometric function

$$F(a, b, c; z) = \sum_{k=0}^{\infty} \frac{(a)_k (b)_k}{(c)_k} \frac{z^k}{k!}$$

with $(a)_k := a(a+1)\cdots(a+k-1)$. The constant D is

$$D = \frac{e^{-\lambda\tau g}}{\Gamma(\lambda\tau)}.$$

If $\lambda\tau = 1$, $\phi(\lambda\tau, S) = 1 - \log S$, and $P_\star(S)$ simplifies to

$$P_\star(S) = \begin{cases} e^{-g} & \text{for } 0 \le S < 1 \\ e^{-g}(1 - \log S) & \text{for } 1 \le S < 2, \end{cases}$$

which is the expression presented in Gilbert and Pollak (1960).

We now formulate the approximation of the membrane potential density, $P(U)$, for correlated excitatory and independent inhibitory input. The neuron's impulse response $h(t)$ is given explicitly in equation 3.4. We fix the PSP amplitude at $A = 1$. Let us first consider the membrane response to the SIP model. Let N_e (N_i) be the number of excitatory (inhibitory) input spike trains and r_e (r_i) the rate of each individual excitatory (inhibitory) spike train. The excitation can be decomposed into two independent Poisson processes (see section 2.1). Let $U_{e_N}(t)$ be the filtered N_eth-order interaction process and $U_{e_1}(t)$ the filtered first-order process. $U_i(t)$ is the filtered inhibitory input spike train with total rate $N_i r_i$. Thus, if $t_k^{e_N}$, $t_k^{e_1}$, and t_k^i denote the times of events in the corresponding pulse trains, we have

$$U_{e_N}(t) = \sum_k N_e h(t - t_k^{e_N})$$

$$U_{e_1}(t) = \sum_k h(t - t_k^{e_1})$$

$$U_i(t) = \sum_k -h(t - t_k^i).$$

Note that we chose the same absolute amplitude for the excitatory and inhibitory synaptic currents. As we are dealing with a linear system, we have $U(t) = U_{e_N}(t) + U_{e_1}(t) + U_i(t)$, and thus $P(U) = (P_{e_N} * P_{e_1} * P_i)(U)$, the convolution product of the densities of the three independent components. We now use Campbell's theorem to obtain the mean and variance of each density. As $\int h(t)\,dt = \tau$ and $\int h(t)^2\,dt = \tau/2$, we have

$$\begin{aligned}
&\mathrm{E}(U_{e_N}) = N_e\alpha\tau = N_e r_e c\tau, && \mathrm{var}(U_{e_N}) = N_e^2\alpha\tau/2 = N_e^2 r_e c\tau/2,\\
&\mathrm{E}(U_{e_1}) = N_e\beta\tau = N_e r_e(1-c)\tau, && \mathrm{var}(U_{e_1}) = N_e\beta\tau/2 = N_e r_e(1-c)\tau/2,\\
&\mathrm{E}(U_i) = -N_i r_i\tau, && \mathrm{var}(U_i) = N_i r_i\tau/2.
\end{aligned}$$

For a large range of parameters, in particular for large excitatory populations, we have $\mathrm{var}(U_{e_N}) \gg \mathrm{var}(U_{e_1}) + \mathrm{var}(U_i)$, and we can approximate the convolution $(P_{e_1} * P_i)(U)$ by a Dirac delta function located at $\mathrm{E}(U_{e_1} + U_i)$. We obtain

$$P(U) \approx P_{e_N}(U - N_e r_e(1-c)\tau + N_i r_i\tau).$$

The density of the membrane potential response of the FR neuron to the MIP model is approximated in a similar manner. Let $U_e(t)$ be the filtered excitatory input. The interacting point processes in the MIP model can be decomposed into N_e+1 independent interaction processes (see section 2.2). Let $U_{e_n}(t)$ be the filtered nth-order interaction process, with rate $\mathrm{B}(n; c, N_e)r_e/c$. The membrane potential of the FR neuron is then given by

$$U(t) = U_e(t) + U_i(t) = \sum_{n=0}^{N} U_{e_n}(t) + U_i(t).$$

The variance of $U_e(t)$ is $\mathrm{var}(U_e) = N_e r_e(1 - c + cN_e)\tau/2$. If the relation $\mathrm{var}(U_e) \gg \mathrm{var}(U_i)$ holds true, we can approximate $P_i(U)$ by a Dirac delta function located at $\mathrm{E}(U_i)$ and write

$$P(U) \approx P_e(U + N_i r_i\tau).$$

In addition, we approximate $U_e(t)$ by $U_{e_{\bar{n}}}(t) = N_e c \sum_k h(t - t_k^{e_{\bar{n}}})$, where $t_k^{e_{\bar{n}}}$ are the times of pulses in the generating process ($w_g(t)$; see section 2.2). Effectively, we let the order of interaction be deterministic and approximate the N interaction processes by a single process with amplitude $\mathrm{E}(n) = N_e c$ and with the same rate r_e/c as the generating process. We then get

$$P(U) \approx P_{e_{\bar{n}}}(U + N_i r_i\tau).$$

The membrane potential density for both input models can thus be approximated by the expression of the shot noise density (see equation B.1), using a linear variable transformation $U = kS - l$. We finally obtain

$$P(U) \approx \frac{1}{k} P_\star\left(\frac{U+l}{k}\right),$$

with an appropriate choice of k, l, and of the parameters of the density function $P_\star$ (see equation B.1). The mean output rate r_o of the FR neuron is then obtained by integrating over the tail of the potential distribution (see equation 3.5) and is expressed in a piecewise manner too. The first two terms are

$$r_o \approx \begin{cases} 1-D & \dfrac{1}{\lambda\tau}\left(\dfrac{\theta+l}{k}\right)^{\lambda\tau} \qquad \text{for } -l \le \theta < k-l \\ 1-D & \left\{ \dfrac{1}{\lambda\tau}\left(\dfrac{\theta+l}{k}\right)^{\lambda\tau} - \displaystyle\int_{k-l}^{\theta} \left(\dfrac{U+l}{k}\right)^{\lambda\tau-1} \left(\dfrac{k}{U+l-k}\right)^{-\lambda\tau} \right. \\ & \quad \left. \cdot F\left(\lambda\tau, \lambda\tau, 1+\lambda\tau; 1-\dfrac{U+l}{k}\right) \right. \\ & \quad \left. \cdot \dfrac{dU}{k} \right\} \qquad \text{for } k-l \le \theta < 2k-l. \end{cases} \tag{B.2}$$

It remains to fix values for λ, k, and l, in the expressions above, with the parameters from the input models. For the SIP model, $\lambda = r_e c$, $k = N_e$, and $l = -N_e r_e (1-c)\tau + N_i r_i \tau$. For the MIP model, $\lambda = r_e/c$, $k = N_e c$, and $l = N_i r_i \tau$. Note that if $N = N_e = N_i$ and $r = r_e = r_i$, the expression $(\theta + l)/k$ simplifies to $\theta/N + rc\tau$ for the SIP model and to $\theta/(Nc) + r\tau/c$ for the MIP model. Hence, the threshold θ and the size of the input population N appear only as the ratio θ/N.

Acknowledgments. This work was supported in part by the Human Frontier Science Program, the Deutsche Forschungsgemeinschaft, and the German-Israeli Foundation for Scientific Research and Development.

References

Aertsen, A., & Gerstein, G. L. (1985). Evaluation of neuronal connectivity: Sensitivity of cross-correlation. *Brain Research, 340*, 341–354.

Azouz, R., & Gray, C. M. (1999). Cellular mechanisms contributing to response variability of cortical neurons in vivo. *J. Neurosci., 19*(6), 2209–2223.

Baker, S. N., Spinks, R., Jackson, A., & Lemon, R. N. (2001). Synchronization in monkey motor cortex during a precision grip task. I. Task-dependent modulation in single-unit synchrony. *J. Neurophysiol., 85*(2), 869–885.

Bernander, Ö., Koch, C., & Usher, M. (1994). The effect of synchronized inputs at the single neuron level. *Neural. Comput., 6*, 622–641.

Bohte, S. M., Spekreijse, H., & Roelfsema, P. R. (2000). The effects of pair-wise and higher-order correlations on the firing rate of a postsynaptic neuron. *Neural. Comput., 12*, 153–179.

Borg-Graham, L. J., Monier, C., & Frégnac, Y. (1998). Visual input evokes transient and strong shunting inhibition in visual cortical neurons. *Nature, 393*, 369–373.

Braitenberg, V., & Schüz, A. (1998). *Cortex: Statistics and geometry of neuronal connectivity* (2nd ed.). Berlin: Springer-Verlag.

Cox, D. R., & Isham, V. (1980). *Point processes*. London: Chapman & Hall.

Das, A., & Gilbert, C. D. (1999). Topography of contextual modulations mediated by short-range interactions in primary visual cortex. *Nature, 399*(6737), 655–661.

DeCharms, R. C., & Merzenich, M. M. (1996). Primary cortical representation of sounds by the coordination of action-potential timing. *Nature, 381*, 610–613.

Deppisch, J., Bauer, H.-U., Schillen, T., König, P., Pawelzik, K., & Geisel, T. (1993). Alternating oscillatory and stochastic states in a network of spiking neurons. *Network, 4*, 243–257.

Destexhe, A., & Paré, D. (1999). Impact of network activity on the integrative properties of neocortical pyramidal neurons in vivo. *J. Neurophysiol., 81*(4), 1531–1547.

Eggermont, J. J., & Smith, G. M. (1995). Rate covariance dominates spontaneous cortical unit-pair correlograms. *Neuroreport, 6*(16), 2125–2128.

Feng, J., & Brown, D. (2000). Impact of correlated inputs on the output of the integrate-and-fire model. *Neural Comput., 12*(3), 671–692.

Feng, J., & Zhang, P. (2001). Behavior of integrate-and-fire and Hodgkin-Huxley models with correlated inputs. *Phys. Rev. E, 63*, 051902:1–11.

Gerstein, G. L., & Aertsen, A. M. H. J. (1985). Representation of cooperative firing activity among simultaneously recorded neurons. *J. Neurophysiol., 54*(6), 1513–1528.

Gilbert, E. N., & Pollak, H. O. (1960). Amplitude distribution of shot noise. *Bell Syst. Tech. J., 39*, 333–350.

Gütig, R., Aertsen, A., & Rotter, S. (2002). Analysis of higher-order neuronal interactions based on conditional inference. Manuscript submitted for publication.

Koch, C. (1999). *Biophysics of computation: Information processing in single neurons*. New York: Oxford University Press.

Kuhn, A., Rotter, S., & Aertsen, A. (2002). Correlated input spike trains and their effects on the leaky integrate-and-fire neuron. *Neurocomputing, 44–46*, 121–126.

Léger, J.-F., Stern, E. A., Aertsen, A., & Heck, D. (2002). Synaptic integration in the cortex shaped by network activity. Manuscript submitted for publication.

Martignon, L., Deco, G., Laskey, K., Diamond, M., Freiwald, W., & Vaadia, E. (2000). Neural coding: Higher-order temporal patterns in the neurostatistics of cell assemblies. *Neural. Comput., 12*, 2621–2653.

Martignon, L., von Hasseln, H., Grün, S., Aertsen, A., & Palm, G. (1995). Detecting higher-order interactions among the spiking events in a group of neurons. *Biol. Cybern., 73*, 69–81.

Matsumura, M., Chen, D., Sawaguchi, T., Kubota, K., & Fetz, E. E. (1996). Synaptic interactions between primate precentral cortex neurons revealed by spike-triggered averaging of intracellular membrane potentials in vivo. *J. Neurosci., 16*(23), 7757–7767.

McCormick, D. A., Connors, B. W., Lighthall, J. W., & Prince, D. A. (1985). Comparative electrophysiology of pyramidal and sparsely spiny neurons of the neocortex. *J. Neurophysiol., 54*, 782–806.

Murthy, V. N., & Fetz, E. E. (1994). Effects of input synchrony on the firing rate of a three-conductance cortical neuron model. *Neural Comput., 6*, 1111–1126.

Nelson, J. I., Salin, P. A., Munk, M. H. J., Arzi, M., & Bullier, J. (1992). Spatial and temporal coherence in cortico-cortical connections: A cross-correlation study in areas 17 and 18 in the cat. *Visual Neurosci., 9*, 21–37.

Nicolelis, M. A. L. (Ed.). (1998). *Methods for neural ensemble recordings*. Boca Raton, FL: CRC Press.

Papoulis, A. (1991). *Probability, random variables, and stochastic processes* (3rd ed.). New York: McGraw-Hill.

Paré, D., Shink, E., Gaudreau, H., Destexhe, A., & Lang, E. (1998). Impact of spontaneous synaptic activity on the resting properties of cat neocortical pyramidal neurons in vivo. *J. Neurophysiol., 79*, 1450–1460.

Rotter, S., & Diesmann, M. (1999). Exact digital simulation of time-invariant linear systems with applications to neuronal modeling. *Biol. Cybern., 81*, 381–402.

Salinas, E., & Sejnowski, T. J. (2000). Impact of correlated synaptic input on output firing rate and variability in simple neuronal models. *J. Neurosci., 20*(16), 6193–6209.

Salinas, E., & Sejnowski, T. J. (2001). Correlated neuronal activity and the flow of neural information. *Nat. Rev. Neurosci., 2*(8), 539–550.

Shadlen, M. N., & Newsome, W. T. (1998). The variable discharge of cortical neurons: Implications for connectivity, computation, and information coding. *J. Neurosci., 18*(10), 3870–3896.

Snyder, D. L., & Miller, M. I. (1991). *Random point processes in time and space* (2nd ed.). New York: Springer-Verlag.

Steinmetz, P., Roy, A., Fitzgerald, P., Hsiao, S., Johnson, K., & Niebur, E. (2000). Attention modulates synchronized neuronal firing in primate somatosensory cortex. *Nature, 404*(6774), 187–190.

Stroeve, S., & Gielen, S. (2001). Correlation between uncoupled conductance-based integrate-and-fire neurons due to common and synchronous presynaptic firing. *Neural Comput., 13*(9), 2005–2029.

Svirskis, G., & Rinzel, J. (2000). Influence of temporal correlations of synaptic input on the rate and variability of firing in neurons. *Biophys. J., 79*, 629–637.

Tiesinga, P. H. E., José, J. V., & Sejnowski, T. J. (2000). Comparison of current-driven and conductance-driven neocortical model neurons with Hodgkin-Huxley voltage-gated channels. *Phys. Rev. E, 62*(6), 8413–8419.

Troyer, T. W., & Miller, K. D. (1997). Physiological gain leads to high ISI variability in a simple model of a cortical regular spiking cell. *Neural Comput., 9*, 971–983.

Tuckwell, H. C. (1988). *Introduction to theoretical neurobiology* (Vol. 2). Cambridge: Cambridge University Press.

van Vreeswijk, C., & Sompolinsky, H. (1996). Chaos in neuronal networks with balanced excitatory and inhibitory activity. *Science, 274*, 1724–1726.

Received May 10, 2002; accepted June 4, 2002.